AIP | Journal of Applied Physics

Ripple dislocation slip in wrinkled gold film deposited on polydimethylsiloxane

C. B. Lin, Y. F. Chuang, Y. H. Liu, Sanboh Lee, and Y. T. Chou

Citation: J. Appl. Phys. **110**, 014313 (2011); doi: 10.1063/1.3606513
View online: http://dx.doi.org/10.1063/1.3606513
View Table of Contents: http://jap.aip.org/resource/1/JAPIAU/v110/i1
Published by the American Institute of Physics.

Ripple dislocation slip in wrinkled gold film deposited on polydimethylsiloxane

C. B. Lin,[1] Y. F. Chuang,[1] Y. H. Liu,[2] Sanboh Lee,[2] and Y. T. Chou[3]
[1]*Department of Mechanical and Electro-Mechanical Engineering, Tam Kang University, Taipei Hsien 25137, Taiwan*
[2]*Department of Material Science and Engineering, National Tsing Hua University, Hsinchu 300, Taiwan*
[3]*Department of Chemical Engineering and Materials Science, University of California, Irvine, California 92697, USA*

(Received 18 April 2011; accepted 28 May 2011; published online 13 July 2011)

The motion of ripple dislocations in a wrinkled thin film of gold deposited on polydimethylsiloxane (PDMS) was investigated. The deposition was made under tensile load along the first direction on the PDMS plate. After the tensile load was released, a ripple pattern and ripple dislocations were formed on the surface. Upon reloading in the second direction, these ripple dislocations were able to slip. At a given tensile load, the speed of slip decreased as the loading time increased, and finally reached a constant value, which was increasing with the applied load. The measured data were interpreted with a dynamic model based on Newton's law of motion. Interaction of ripple dislocations was also observed. It was shown that a pair of positive and negative ripple dislocations of equal strength could annihilate each other or form a dipole, depending on the magnitude of the applied load. © *2011 American Institute of Physics*. [doi:10.1063/1.3606513]

I. INTRODUCTION

Surface instability often occurs on liquid and soft solid films and leads to self-assembled structure formation due to van der Waals interaction,[1] thermal gradient,[2] electric field,[3] residual stress,[4,5] solvent gradient,[6] etc. As thin films have been widely applied in low-dimensional structures, the morphological evolution in thin film became a critical phenomenon in the choice of micro- and nanofabrication techniques for microelectromechanical and nanoelectromechanical structures. As a result, the surface evolution in thin films due to buckling has been studied extensively in the past decade,[6–10] with emphasis on propagation of surface ripples and buckles. More recently, ripple dislocations were observed and studied.[4,11–14] Lin *et al*.[4] found that the presence of ripple dislocations would affect the crack propagation in a wrinkled gold film deposited on polydimethylsiloxane (PDMS). Ohzono and Shimomura[13] observed the ripple dislocation slip and annihilation on the surface of a Pt-coated elastomer under compression. They also observed ripple dislocation motion and interaction in the Pt-coated elastomer subjected to gradual change in the compression direction.[14] However, the relationship between the strain field and dislocation slip remains unexplored. In this article, we present a new study on motion and interactions of ripple dislocations in the wrinkled gold film on PDMS.

II. EXPERIMENT

The procedure of sample preparation was similar to that given in the previous work.[4] Briefly, the PDMS gels were mixed with curing agents at a weight percent ratio of 15:1 and placed in a vacuum chamber of 10^{-2} Torr to eliminate the bubbles. The mixture was coated on a clean Si wafer of 4 in. diameter using a spin coater. After dried, the PDMS plate with 0.2 mm thickness was detached from the Si wafer and cut into samples of dog-bone shape with a gauge length of 8 mm. Each sample was elongated under the tensile load, and a thin film of gold with thickness 4 Å was deposited on the elongated PDMS sample at room temperature using a Hitachi E-1010 sputter under a pressure less than 10 Pa. After the tensile load was released, the ripple pattern and ripple dislocations were formed on the sample surface due to buckling, as observed under an Olympus B071 optical microscope. The ripples appear to be lined up perpendicular to the direction of tensile load applied during the formation of the ripple pattern. Hereafter, we will refer to it as the first load direction [see Fig. 1(a)]. Sometimes, positive ripple dislocation A and negative dislocation B were also observed in a curly ripple pattern, as shown in Fig. 1(b).

To study the motion of ripple dislocations, the sample containing the defects was again subjected to a tensile load along a second direction inclined by an angle θ from the first load direction [Fig. 1(a)]. While under the second load the ripple dislocations began to move, and their positions were recorded in sequence using an Olympus optical microscope with a charge coupled device camera. Note that the ripple dislocations observed in this study have a shape of letter Y. We may call them the Y-shaped ripple dislocations in difference from the simple ripple dislocations (the T-shaped) that are also commonly observed.[4,11,12]

III. RESULTS

Unlike the case of lattice dislocations,[15] slip of ripple dislocations is not well known. In this study we are able to see such a process in the thin gold film.

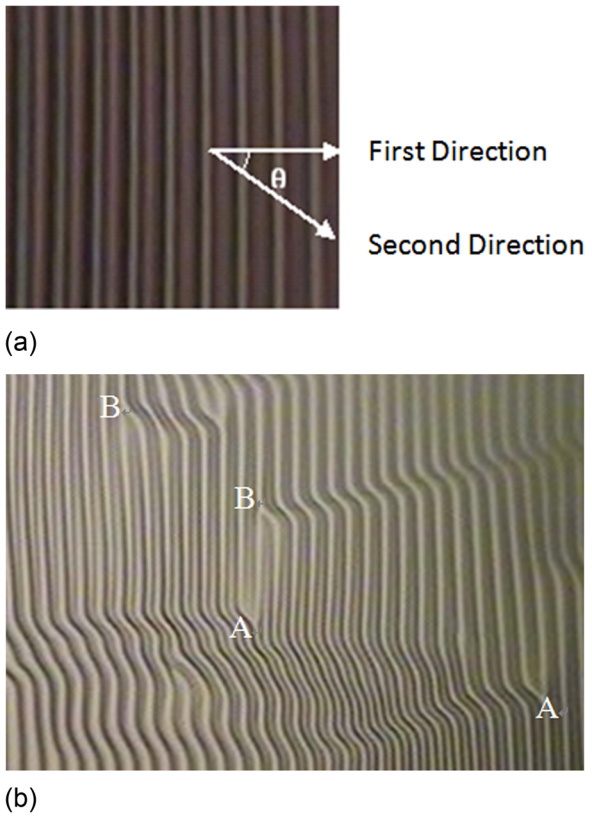

FIG. 1. (Color online) Micrographs showing (a) the loading directions in reference to the ripple lines. The first load is released for the pattern formation and the second is applied for the motion of ripple dislocations, and (b) a pair of positive dislocation A and negative dislocation B in a ripple lattice of the Au-PDMS system prior to reloading.

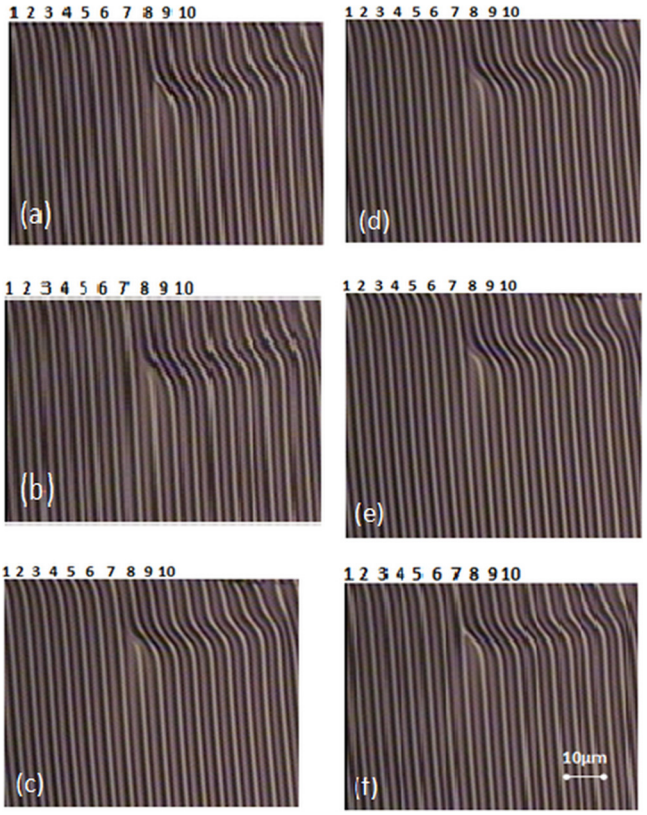

FIG. 2. (Color online) Sequential micrographs showing the motion of a ripple dislocation in the sample under a tensile load of 245 mN at $\theta = 37°$: (a) 0 s; (b) 0.2 s; (c) 0.5 s; (d) 0.8 s; (e) 1 s; and (f) 3 s.

A. Slip of ripple dislocations

The sample was elongated to 118% along the first load direction, unloaded, and then reloaded to 245 mN along the second direction at $\theta = 37°$. Under the second tensile load, the ripple dislocation was able to move, as shown in Fig. 2. In Fig. 2(a), the load is not yet applied ($t = 0$); the dislocation is located at the eighth ripple line. It is noted that the ripples in the left region of the dislocation are straight, whereas those in the right are distorted and curved. As the loading time increases, the straight seventh ripple in the left of the dislocation begins curving. The Y-shaped dislocation at ripple eight now becomes unstable and one of its arms is dislodged to form a T-shaped dislocation. Under the stress, this intermediate product continues to be bent toward ripple seven [Figs. 2(b)–2(e)]. And finally the two rejoin to form a Y-shaped dislocation at the new location [Fig. 2(f) at $t = 3$ s]. The ripple dislocation thus has moved by a distance between the two neighboring ripples, similar to the case of lattice dislocation slip by a Burgers vector.[15]

B. Dynamics of ripple dislocation motion

Using the controlled experimental setup we proceeded to obtain more data on the motion of ripple dislocations as shown in Figs. 3(a) and 3(b). We found that the speed of slip decreased with the increase of loading time until it reached a constant value. The trend was observed for samples tested under different loads [Fig. 3(b)]. On the other hand, the steady state slip speed was found to increase with increasing load. However, unlike the case of lattice dislocations,[15] multiplication of ripple dislocation was not observed even under very high stress. This is because that ripple dislocation loop is absent in the thin film case.

The experimental data of displacement at time t under different applied loads are shown in Fig. 3(a) by the solid circles, where the samples are elongated to 112%, unloaded, and then reloaded at different magnitudes along the second direction. For a given time, the displacement increases with applied load. For a given load, the slope of each curve is constant at the long times.

To analyze the dynamics of the moving ripple dislocation, we treat the unit length dislocation as a particle with an effective mass m^* in a viscous composite of viscous coefficient η. Under the action of the applied load F, it sets into motion governed by the Newton's law,

$$m^* \frac{d^2x}{dt^2} + \eta \frac{dx}{dt} = f, \tag{1}$$

where the first term on the left-hand side of the equation is the inertia force and the second is the viscous drag force. The total internal force f on the unit dislocation is composed of two parts given by

$$f = f_{\text{appl}} + f_{\text{odf}}, \tag{2}$$

where f_{appl} is the force due to the applied load F, and f_{odf} is the net force on the moving dislocation due to all other

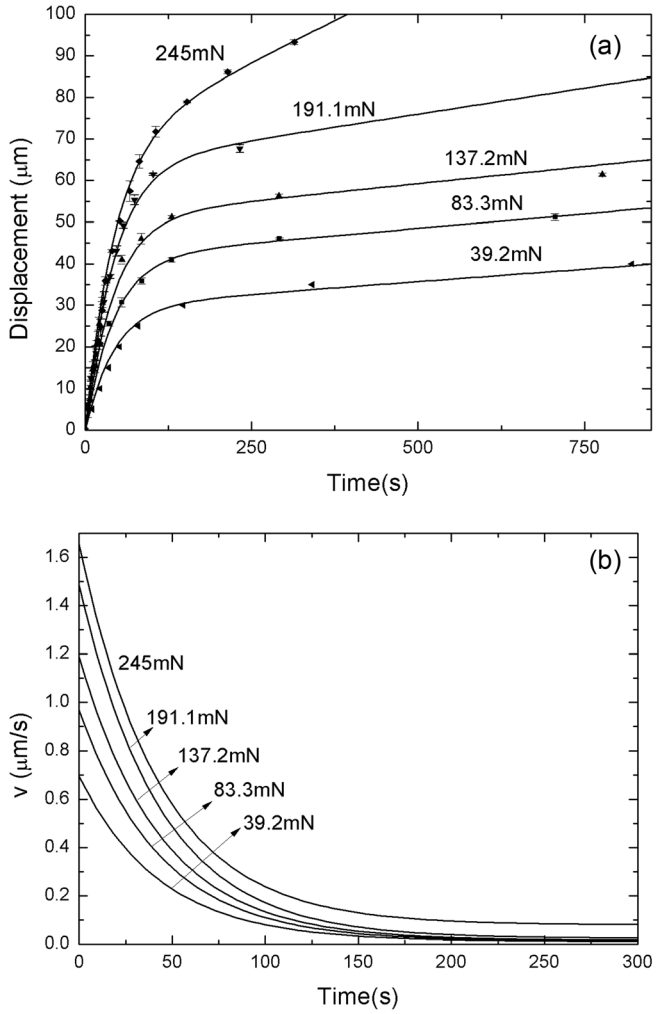

FIG. 3. Plots of (a) displacement vs time and (b) velocity vs time at different loads. The continuous lines and solid circles are from theoretical predictions and experimental data, respectively.

defects in the neighborhood. The latter is assigned as positive (+) if it acts in the same direction of the former, and negative (−) if in the opposite direction.

Equation (1) can be integrated giving

$$\frac{dx}{dt} = v = \frac{f}{\eta} + \lambda \exp(-\eta t/m^*) \tag{3}$$

and integrating Eq. (3), we obtain

$$x = \frac{f}{\eta} t + \frac{m^* \lambda}{\eta} [1 - \exp(-\eta t/m^*)], \tag{4}$$

TABLE I. The estimated values of f/m^*, η/m^* and λ used in evaluating x from Eq. (4).

F (mN)	f/m^* (10^{-4} m/s^2)	η/m^* (s^{-1})	λ (μm/s)
39.2	2.76	0.023	0.6831
83.3	3.22	0.023	0.9545
137.2	3.795	0.023	1.173
191.1	5.75	0.023	1.4605
245	18.4	0.023	1.5755

where λ is the integration constant determined by the initial condition. It is seen from Eq. (3) that at $t = \infty$, $v = f/\eta$. That is, at the steady state, the velocity of the ripple dislocation is linearly proportional to the total internal force on the defect.

To compute the numerical values of v and x from Eqs. (3) and (4), we need the numerical data of the parameters f/m^*, η/m^*, and λ, and none of these data are known at present. In an effort to understand the dynamic process, we adopt the best fitting technique on a computer. The results are shown in Figs. 3(a) and 3(b). The computer fitted data for the parameters are given in Table I, and the effectiveness of the fitting technique is seen from the constancy of the η/m^* values in the third column of the table.

C. Dislocation interaction and annihilation

When a positive lattice dislocation meets a negative lattice dislocation, they may interact and disappear.[16] Such an interaction was also observed for ripple dislocations. Figure 4

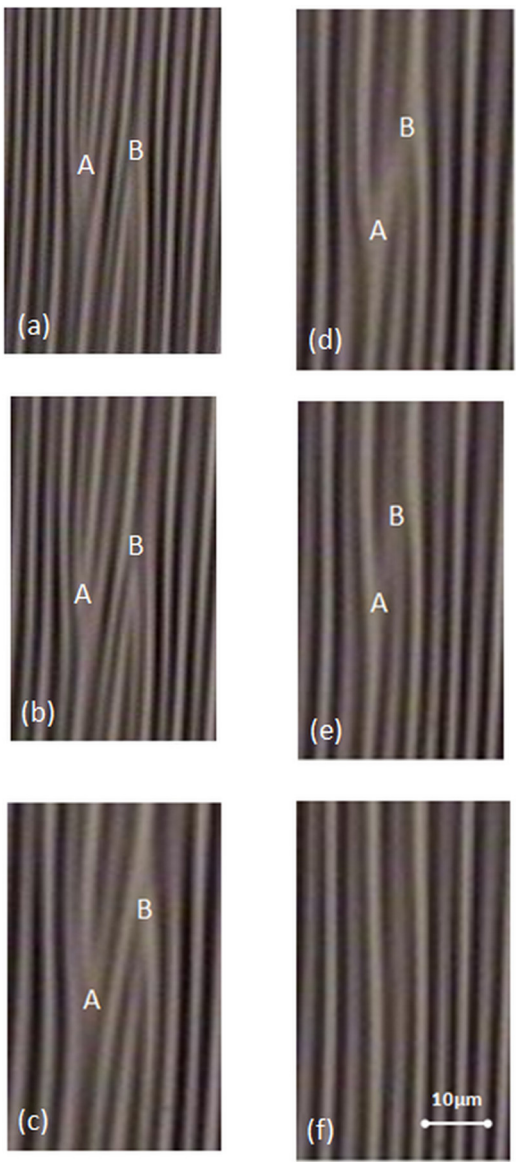

FIG. 4. (Color online) Sequential micrographs showing the annihilation of ripple dislocations under a tensile load of 98 mN at $\theta = 20°$: (a) 0 s; (b) 27 s; (c) 47 s; (d) 49 s; (e) 51 s; and (f) 54 s.

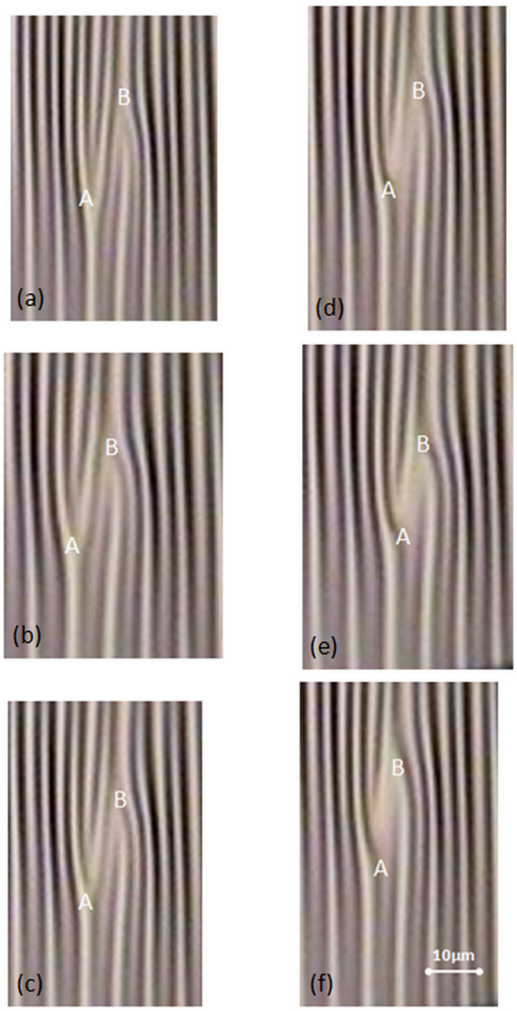

FIG. 5. (Color online) Sequential micrographs showing the formation of a ripple dislocation dipole under a tensile load of 27.4 mN at $\theta = 37°$: (a) 0 s; (b) 325 s; (c) 340 s; (d) 345 s; (e) 360 s; and (f) 383 s.

shows a sequential recording of dislocation annihilation, when the sample is under a tensile load of 98 mN at $\theta = 20°$. The positive ripple dislocation A is separated from the negative ripple dislocation B by two ripple lines as shown in Fig. 4(a). Both dislocations are closer as the time increases. Finally, the two and two ripple lines in between disappear, and the ripples retain the normal pattern of straight lines. Although the ripple dislocation annihilation was also observed by Ohzono and Shimomura,[14] they did not find the disappearance of ripple stripes between both positive and negative dislocations. This difference may affect the relation between strain field and dislocation slip. On the other hand, if the load were not sufficiently high, dislocation annihilation would be prohibited. Figure 5 illustrates a sequence of micrographs showing the motion of ripple dislocations under a tensile load of 27.4 mN at $\theta = 37°$. When the positive and the negative ripple dislocation approach each other under the action of load, they were not annihilated but instead united to form a ripple dislocation dipole.

D. Comparison between lattice dislocation and ripple dislocation

At this early stage of exploration of ripple dislocations, it seems useful to clarify the differences and similarities between the lattice dislocation and the ripple dislocation. Basically, the former is a two-dimensional microdefect and the latter is a one-dimensional macrodefect.[4,11–14] Thus, one would not expect that the ripple dislocation have the screw component as the lattice dislocation does. Also its climb motion (in parallel to the ripple line) is not step-wise but continuous. In dynamics, the two defects behave differently. For a ripple dislocation in a viscous–elastic composite, the velocity at the steady state is linearly proportional to the total internal force [Eq. (3)], whereas for a lattice dislocation in an elastic medium, its velocity–force relationship obeys the power law of Johnston and Gilman.[16]

On the other hand, there are close similarities between the two defects, especially between their edge components. The two are geometrically similar,[17] and both have the internal stress field.[4,13] We have shown the similar process of dipole formation and annihilation (Fig. 4). We also observed the similar slip processes that involve disjoining, displacing, and rejoining (Fig. 3).

IV. SUMMARY

We showed that a ripple dislocation would slip in the ripple lattice under loading. The ripple stripes and ripple dislocations were observed on the surface of a wrinkled gold film on a PDMS plate. The speed of slip varies with the applied load, increasing as the load increases. Its dynamics obeys the Newton's law. The annihilation of a pair of positive and negative ripple dislocations was observed at a sufficiently high load. Under a lower load, they formed a dipole.

ACKNOWLEDGMENTS

This work was supported by the National Science Council, Taiwan.

[1]A. Sharma, Eur. Phys. J. E **12**, 397 (2003).
[2]J. Peng, H. Wang, B. Li, and Y. Han, Polymer **45**, 8013 (2004).
[3]N. E. Voicu, S. Harkema, and U. Steiner, Adv. Funct. Mater. **16**, 926 (2006).
[4]C. B. Lin, C. C. Lin, S. Lee, and Y. T. Chou, J. Appl. Phys. **104**, 016106 (2008).
[5]C. C. Lin, F. Yang, and S. Lee, Langmuir **24**, 13627 (2008).
[6]K. F. Chou, S. Lee, and J. P. Harmon, Macromolecules **36**, 5683 (2003).
[7]J. Munoz-Garcia, M. Castro, and R. Cuerno, Phys. Rev. Lett. **96**, 086101 (2006).
[8]P. F. A. Alkemade, Phys. Rev. Lett. **96**, 107602 (2006).
[9]Q. M. Wei, J. Lian, W. Lu, and L. M. Wang, Phys. Rev. Lett. **100**, 076103 (2008).
[10]Q. M. Wei, J. Lian, L. A. Boatner, L. M. Wang, and R. C. Ewing, Phys. Rev. B **80**, 085413 (2009).
[11]F. Katzenberg, Macromol. Mater. Eng. **286**, 26–29 (2001).
[12]K. Efimenko, M. Rackaitis, E. Manias, A. Vaziri, L. Mahadevan, and J. Genzer, Nat. Mater. **4**, 293 (2005).
[13]T. Ohzono and M. Shimomura, Phys. Rev. B **69**, 132203 (2004).
[14]T. Ohzono and M. Shimomura, Phys. Rev. E **73**, 040601 (2006).
[15]J. J. Gilman and W. G. Johnston, in *Dislocations and Mechanical Properties of Crystals*, edited by J. C. Fisher, W. G. Johnston, R. Thomson, and T. Vreeland, Jr. (Wiley, New York, 1957), p. 116.
[16]W. G. Johnston and J. J. Gilman, J. Appl. Phys. **30**, 129 (1959).
[17]J. P. Hirth and J. Lothe, *Theory of Dislocation*, 2nd Ed. (Wiley, New York, 1982), p. 19.